Structure of Heat-Induced β-Lactoglobulin Aggregates and their Complexes with Sodium-Dodecyl Sulfate

Jin-Mi Jung,[†,‡] Gabriela Savin,[‡] Matthieu Pouzot,[‡] Christophe Schmitt,[‡] and
Raffaele Mezzenga*,[†,‡]

*Department of Physics, University of Fribourg, Perolles, Fribourg, CH-1700, Switzerland, and Department
of Food Science and Technology, Nestlé Research Center, Vers-Chez-Les-Blanc, Lausanne 26,
CH-1000, Switzerland*

We report on the conformation of heat-induced bovine β-lactoglobulin (βlg) aggregates prepared at different pH conditions, and their complexes with model anionic surfactants such as sodium dodecyl sulfate (SDS). The investigation was carried out by combining a wide range of techniques such as ultra small angle light scattering, static and dynamic light scattering, small angle neutron scattering, small-angle X-ray scattering, electrophoretic mobility, isothermal titration calorimetry (ITC) and transmission electron microscopy. Three types of aggregates were generated upon heating βlg aqueous dispersions at increasing pH from 2.0 to 5.8 to 7.0: rod-like aggregates, spherical aggregates, and worm-like primary aggregates, respectively. These aggregates were shown not only to differ for their sizes and morphologies, but also for their internal structures and fractal dimensions. The main differences between aggregates are discussed in terms of the ionic charge and conformational changes arising for βlg at different pHs. The formation of complexes between SDS and the various protein aggregates at pH 3.0 was shown to occur by two main mechanisms: at low concentration of SDS, the complex formation occurs essentially by ionic binding between the positive residues of the protein and the negative sulfate heads of the surfactant. At complete neutralization of charges, precipitation of the complexes is observed. Upon further increase in SDS concentration, complex formation of SDS and the protein aggregates occurs primarily by hydrophobic interactions, leading to (i) the formation of an SDS double layer around the protein aggregates, (ii) the inversion of the total ionic charge of each individual protein aggregate, and (iii) the complete redispersion of the protein aggregate−SDS complexes in water. Remarkably, the SDS double layer around the protein aggregates provides an efficient protective shield, preventing precipitation of the aggregates at any possible pH values, including those values corresponding to the isoelectric pH of the aggregates.

1. Introduction

β-Lactoglobulin (βlg) is a globular protein, abundantly contained in bovine milk, which has attracted much attention for its potential use in the food industry. In its "native" monomer form, it has 162 amino acid residues with eight antiparallel β-sheets, one α-helix chain, and a molar mass of 18.3 kDa.[1,2] In particular, each monomer has an internal core with predominantly hydrophobic residues inside, while the hydrophilic amino acids are mostly located in the surface. The protein contains two disulfide bonds and one free sulfhydric group, whose reactivity is pH-dependent (pK_a = 8.3), and carries 20 basic amino acids per monomer, which at pH = 2.3 corresponds to a maximum of proton charges at the protein surface. At neutral pH, the quaternary structure of βlg is dimeric in equilibrium with the monomeric form, while at pH 2 the monomeric form predominates. The monomer−dimer equilibrium depends on the protein concentration, ionic strength, and temperature.[3,4]

When the temperature is increased above 70 °C, βlg partially denatures and aggregates, leading to the formation of soluble aggregates if the protein concentration c is below the critical gelation concentration c_{gel} or to the formation of a continuous network (also referred as gel) if $c > c_{gel}$.[5−9] When soluble aggregates are generated, the kinetics of the aggregation is strongly dependent on the temperature of the heat treatment and the protein concentration. The ionic strength and the pH influence not only the kinetics but also the structure of the aggregates formed. For example, at neutral pH and high ionic strength the dispersion becomes turbid[10−12] upon heating, while at pH 2.0 and low salt concentrations it remains transparent.[13−15] A thiol-catalyzed aggregation mechanism, analogous to free radical-induced polymerization, was proposed by Roefs and de Kruif for βlg heated at 65 °C at neutral pH and low ionic strength.[16] At temperatures higher than 80 °C, noncovalent interactions become of increasing importance and the aggregation process is dominated by both interchange of disulphide bonds and hydrophobic interactions.[17−19] In the case of pH close to the isoelectric pH (IEP) of the "native" protein dimer (IEP = 5.1), the interchange of disulphide bonds is less prone to occur, and the aggregation process is dominated by the electrostatic attractions and hydrophobic interactions.[20−22] Below the IEP, at pH 2, the very low reactivity of the sulfhydric group inhibits formation of covalent bonds, the electrostatic repulsions are substantial, and aggregates based on noncovalent interactions (ionic, dipole, van der Waals, hydrophobic) are formed.[23]

The understanding of aggregation of proteins has made a considerable progress by the introduction of the concept of

* To whom correspondence should be addressed. Phone: +41 (0)26 300 9066 (University of Fribourg); +41 (0)21 785 8078(Nestlé Research Center). Fax: +41 (0)26 300 9747 (University of Fribourg); +41 (0)21 785 8554 (Nestlé Research Center). E-mail: raffaele.mezzenga@unifr.ch; raffaele.mezzenga@rdls.nestle.com.
† University of Fribourg.
‡ Nestlé Research Center.

fractals.[24−26] According to this concept, the complex structure of aggregated particles can be described by a fractal dimension d_f, indicating the relation between the number of particles in the aggregates and its typical size, $N \approx R^{d_f}$. The value of d_f is not necessarily an integer number and in principle can have any value between 1 and 3. A dimensionality of 1 is expected for rod-like aggregates, while $d_f = 3$ should be observed for compact sphere-like aggregates.

In the present study, the relevance of the fractal concept for description of bovine βlg aggregates prepared at very low ionic strength and three different values of pH, below, close to, and above the IEP is investigated using a combination of different scattering techniques such as light scattering (LS), small-angle X-ray scattering (SAXS), small-angle neutron scattering (SANS), and transmission electron microscopy (TEM). Full characterization of the structure of globular protein self-assemblies by combined light scattering and X-ray scattering has been done so far only for ovalbumin at pH 7[10] and βlg at pH 2 and 7 at relatively high ionic strength. In the case of βlg aggregates, it has been found that the fractal dimension remains close to 2, but the density increases when the pH approaches the IEP.[10,11]

The diversity on the structure of βlg aggregates was further exploited in order to investigate the interactions with a model anionic surfactant, sodium dodecyl sulfate (SDS). Previous studies have shown that ionic surfactants may bind to protein molecules through a variety of different physicochemical mechanisms.[27−29] For example, the ionic head groups of surfactants may bind to oppositely-charged groups on the protein surface through electrostatic attraction; alternatively, the non-polar tail groups of surfactants may bind to nonpolar regions on the protein surface through hydrophobic interactions. Surfactants may bind to proteins either as individual monomers or as micelle-like clusters, depending on the surfactant concentration and the nature of interactions.[30] Once a surfactant has bound to a protein, it may either stabilize or destabilize the protein structure and it may either promote or hinder protein aggregation, depending on the surfactant type, surfactant concentration, and environmental conditions. Furthermore, perturbations of the molecular characteristics of globular proteins by interactions with surfactants may lead to changes in their ability to bind other molecules, to self-associate, and to adsorb to interfaces, thereby altering their functional characteristics.[31,32]

Apparently, the effects of SDS on native βlg[33] at different pHs depend on both the charge of the protein and the surfactant and on the surfactant concentration. A small amount of SDS may enhance the helix content of unfolded protein and eventually the protein stability.

The present paper focuses on βlg aggregates−SDS complexes in which protein−surfactant interactions are mainly electrostatic in nature. Particular attention in the study is addressed to the effect of surfactant concentration on the physical properties of the βlg aggregate-SDS complexes.

2. Materials and Methods

2.1. Materials. *2.1.1. Preparation of β-Lactoglobulin Solutions.* BioPURE-betalactoglobulin (lot JE 003-6-922, from 23-05-2005) was obtained from Davisco Foods International, Inc. (Le Sueur, MN). The powder consisted of 97% protein on a dry basis, among which 95.9% of β-lactoglobulin (variant A, 55.6%; variant B, 44.4%) as determined by HPLC (data not shown). To remove non-"native" proteins, the following procedure was set up. First, the protein powder was dissolved in MilliQ water at 10 wt % concentration and the solution was adjusted to pH 4.6 using a 1 M HCl solution. Then, it was centrifuged at 15000 rpm over a period of 15 min at 20 °C using Sorvall Evolution RC

Table 1. Mineral Composition before and after Acid-Dialysis of β-Lactoglobulin Powder

In mg/100 g	initial β-lactoglobulin	dialysed and freeze-dried β-lactoglobulin
Ca	23	<2
Mg	2.1	<0.1
Na	763	<6
K	11	<8
P	62	<25
Cl	<20	4130[a]

[a] The high content in chloride ions comes from the dialysis step against water at pH 2.0 adjusted with 1 M HCl.

Table 2. Experimental Conditions Applied To Obtain Three Different Aggregate Shapes after Heat Treatment of β-Lactoglobulin

	protocol 1	protocol 2	protocol 3
βlg concentration (% wt)[a]	4[b]	1	1
pH	2.0	5.8	7.0
temperature (°C)	90	85	85
heating time (min)	300	15	15
conversion rate (%)	82 ± 5	85 ± 2	83 ± 4

[a] The used monomer concentration was below the critical gelation concentration of the three different types of aggregates.[10,35,39,40] [b] Previous studies on heat-induced fibrillar aggregation of βlg at pH 2.0 and at low ionic strength showed that a higher initial monomer concentration leads to increased formation of fibrils. To have a conversion rate of approximately 80% in the three protocols, at pH 2.0, an initial monomer concentration equal to 4 wt % was required.[41] The samples prepared at pH 2.0 were subsequently diluted to a final protein concentration of 1 wt %. The dilution was done to facilitate comparison of the results obtained from experiments performed at different pHs but starting with the same initial protein concentration.

High Speed Centrifuge (Rotor SLA-1000), and the supernatant was recovered and adjusted to pH 2 using a 1 M HCl solution. To further remove possible residual traces of insoluble proteins, the supernatant was filtered through a 0.22 μm Millipore filter. To remove traces of ions that affect βlg aggregation,[34] the filtered protein solution was dialyzed first against pH 2 MilliQ water and second against MilliQ water, using a Spectra-Por Dialysis Membrane 1, with a MWCO of 6000−8000 Da (Spectrum Laboratories, Inc., CA). Dialysis tubes were previously boiled for 10 min in demineralized water in the presence of 1 mM EDTA and extensively rinsed with demineralized water. The volume ratio between the solvent and the protein solution was kept constant at around 40 during the dialysis. The dialysis was performed at 4 °C with at least 4 h between the dialysis buffer changes. After dialysis, the solution was adjusted back to pH 2. The mineral composition of β-lactoglobulin was determined before and after dialysis by ICP-EAS (Table 1). For storage, the solution was freeze-dried and placed in a desiccator at room temperature. All the experiments were carried out using this dialyzed and freeze-dried β-lactoglobulin powder.

2.1.2. Preparation of Thermally Induced β-Lactoglobulin Aggregates. Dialyzed and freeze-dried β-lactoglobulin powder was dissolved in MilliQ water at room temperature, centrifuged at 10800 g over a period of 1 h at 20 °C using a Sorvall RC3C Plus Centrifuge (DuPont, Newtown, CT), adjusted to the proper pH, and filtered through a 0.45 μm Millipore filter before heat-treatment. Three distinct experimental conditions were applied to obtain three structures of protein aggregates. These procedures were adapted from existing protocols[5,13,35−37] and are given in Table 2. The usual protocol followed to produce rod-like aggregates is heat treatment of diluted solutions of monomer at 80 °C during 10 h, but we chose to increase the temperature to 90 °C and to decrease the heating time because this still leads to rod-like aggregates and improves the conversion rate.[5,38] Glass tubes were filled with 13 mL of β-lactoglobulin solution 1% wt, hermetically sealed, and heated in a water bath without stirring. Three shapes of aggregates (rod-like, spherical, and worm-like) were obtained by varying the pH of the protein solution before heat treatment, from pH 2.0 to 5.8 and to 7.0, respectively. After heat treatment, glass tubes were

immediately cooled by immersion in ice−water mixtures to quench the aggregation process.

2.1.3. Determination of Conversion Rate. The initial concentration of native β-lactoglobulin was checked by UV spectroscopy at 278 nm, using a Uvikon 810 spectrophotometer (Kontron Instruments, Flowspec, Switzerland). The extinction coefficient for the calibration was determined experimentally using known concentrations of β-lactoglobulin solutions at pH 2.0, where the β-lactoglobulin is present as monomer (data not shown). The determined value, $\epsilon_{278} = 0.8272$ L·cm^{-1}·g^{-1} is in agreement with the value determined by Arnaudov et al.[14]

The conversion rate was also determined by UV spectroscopy at 278 nm, following the protocol of Veerman et al.[5] The heat-treated solution was diluted with MilliQ water and precipitated at pH 4.6 and centrifuged at 22000 *g* during 15 min at 20 °C using Sorvall Evolution RC High Speed Centrifuge (Rotor SM24). The absorbance of the supernatant was read at 278 nm, yielding the concentration of nonaggregated β-lactoglobulin. The difference between the initial β-lactoglobulin concentration and the nonaggregated β-lactoglobulin concentration gives the amount of aggregated β-lactoglobulin, its ratio over the initial concentration being referred as the conversion yield.

2.1.4. Complex Formation between β-Lactoglobulin Aggregates and SDS. Complex formation between β-lactoglobulin aggregates and the model anionic surfactant sodium dodecyl sulfate (SDS) was investigated. SDS was supplied by Sigma Aldrich and had a purity >99%. To generate complexes, the solution of β-lactoglobulin aggregates was adjusted to pH 3.0, where the aggregates bear an overall positive charge. The solution of SDS was also adjusted to pH 3.0, without affecting the sulfate negative charge. To follow the complexation, a titration experiment was performed. A total of 10 mL of a solution of β-lactoglobulin aggregates at 0.1 wt % and adjusted to pH 3 was prepared. A solution of SDS at 0.1 wt % and adjusted to pH 3.0 was prepared and used to titrate (mL increment) the solution of β-lactoglobulin aggregates. The solution of β-lactoglobulin aggregates was gently stirred during the titration and an equilibration time of 5 min was set between each addition of SDS.

2.2. Methods. *2.2.1. Transmission Electron Microscopy.* β-Lactoglobulin aggregates and their complexes were observed by transmission electron microscopy (TEM). A drop of the diluted solution (0.1−1 wt % final concentration) was casted onto a carbon support film on a copper grid. The excess solution was removed after 30 s using a filter paper. Contrast to electrons was achieved by negative staining by adding a droplet of phosphotungstic acid solution 1 wt % (PTA, pH 7, Sigma-Aldrich, Switzerland) onto the grid, over a period of 15 s, after deposition of β-lactoglobulin aggregates solution. Any excess of staining agent was removed again by a filter paper. Electron micrographs were acquired on a CCD camera using a Philips CM100 Biotwin transmission electron microscope operating at 80 kV.

2.2.2. Scattering Experiments. The structure of β-lactoglobulin aggregates was characterized by scattering experiments. By combining three radiation sources, that is, light, X-rays, and neutrons, it was possible to cover a wide range of length scales, going from several nm to several μm. Therefore, different levels of structural organizations could be covered.

2.2.2.1. Ultra Small Angle Light Scattering. A CCD camera based light scattering setup, developed within the Soft Condensed Matter group, University of Fribourg, Switzerland, was used to perform simultaneous static and dynamic measurements at ultra small angles (0.08−10°), which corresponds to scattering vectors in the range 185−23000 cm^{-1}. For details of the design of the ultra small angle light scattering instrument, see refs 42 and 43.

2.2.2.2. Static and Dynamic Light Scattering. Static and dynamic light scattering were performed on solutions of β-lactoglobulin aggregates at 20 °C. The range of investigated concentrations was between 0.2 and 1 wt %. Prior to the measurements, all solutions were filtered through 0.45 μm Millipore membrane filters. Depending on the turbidity of the sample, two pieces of equipment were used. Transparent systems were investigated using ALV-5000 fast correlator in combination with

a monomode fiber compact goniometer system and an argon-ion laser Coherent Innova 308 ($\lambda = 532$ nm). Turbid systems were investigated by 3D-cross correlation light scattering[44] using a 3D Flex correlator in combination with a monomode fiber goniometer system and a Diode Laser with a wavelength of 632.8 nm (TUI Optics). The range of scattering vectors covered was 3×10^{-3} nm^{-1} < q < 10^{-2} nm^{-1} with $q = 4\pi n/\lambda_0 \sin(\theta/2)$, λ_0 ($\lambda = \lambda_0/n$), n and θ being, respectively, the light source wavelength in vacuum, the solvent refractive index, and the angle between the detector and the incident beam. Measurements were made in an angular region from 45 to 120° with a step of 5°. Freshly distilled and filtered toluene was used to calibrate the instruments. The Rayleigh ratios for toluene are 3.16×10^{-5} cm^{-1} at 532 nm and 1.02×10^{-5} cm^{-1} at 632.8 nm. A refractive index increment of 0.189 mL·g^{-1} was used.[38]

2.2.2.3. Small Angle X-ray Scattering. Small angle X-ray measurements (SAXS) were made under vacuum using a Philips PW 3830 X-ray generator operating at 40 kV and 50 mA, an Anton Paar SAXSess slit camera and combination of focusing mirrors with a block collimator and an imaging plate detection system. The q range covered was 0.08 < q < 6 nm^{-1}.

The solutions were measured at a concentration of 1% wt. The scattering intensity was normalized by the concentration and exposure time. The scattering intensity was obtained by subtracting the background signals following the equation:

$$I_{\text{SAXS}} = \frac{I_{\text{sample}} - I_{\text{solvent}}}{I_{\text{solvent}} - I_{\text{empty}}} \quad (1)$$

2.2.2.4. Small Angle Neutron Scattering. To obtain sufficient contrast, the small angle neutron scattering (SANS) measurements were performed on aggregates prepared in D$_2$O. βlg was directly dissolved in D$_2$O together with the required amount of DCl or NaOD and heat denatured as described before. All samples were measured at a temperature of 20 °C. When merging light scattering data measured in H$_2$O with SANS data measured in D$_2$O, the influence of solvent should be taken into account. However, previous studies[7,13] showed that although the aggregation process is slower in D$_2$O, there is no significant difference between the structure of βlg aggregates prepared in the two solvents. SANS measurements were performed at the SANS II facility at the Swiss neutron source SINQ at the Paul Scherer Institute, Switzerland. Quartz cells (1 and 2 mm) from Helma were used. Combinations of different wavelengths (4.55 and 6.37 Å^{-1}), sample-to-detector distances (1.2−6 m), and collimation length (2−6 m) resulted in a q range of 0.04−3 nm^{-1}. The raw spectra were corrected for background from the solvent (D$_2$O), sample cell, and electronic noise by conventional procedures. Furthermore, the two-dimensional isotropic scattering spectra were corrected for detector efficiency by dividing with the incoherent scattering spectra of pure water and azimuthally averaged.[45,46]

2.2.3. Electrophoretic Mobility. The complex formation between β-lactoglobulin and SDS was followed by measuring the electrophoretic mobility, using a Nanosizer ZS instrument equipped with backscattering detection at an angle of 173° (Malvern Instruments, Worcestershire, UK). The sample was carefully filled into a disposable ζ-potential folded capillary cell (DTS1060) to avoid air bubble formation. Electrophoretic mobility was measured by performing an electrophoresis experiment on the sample and measuring the velocity of the particles using laser doppler velocimetry (LDV). It was calculated according to the Smoluchowsky equation, assuming that the particle dimensions are greater than the electronic double layer thickness and independently from their shape

$$\nu = \mu_{\text{E}} \times E \quad (2)$$

with ν, velocity of the particles in the solution (μm·s^{-1}), E, the applied electrical field of the measuring cell (V·cm^{-1}), and μ_{E}, electrophoretic mobility of the particles (μm·cm·V^{-1}·s^{-1}).

2.2.4. Isothermal Titration Calorimetry. The enthalpy changes during the complex formation between the β-lactoglobulin aggregates and the
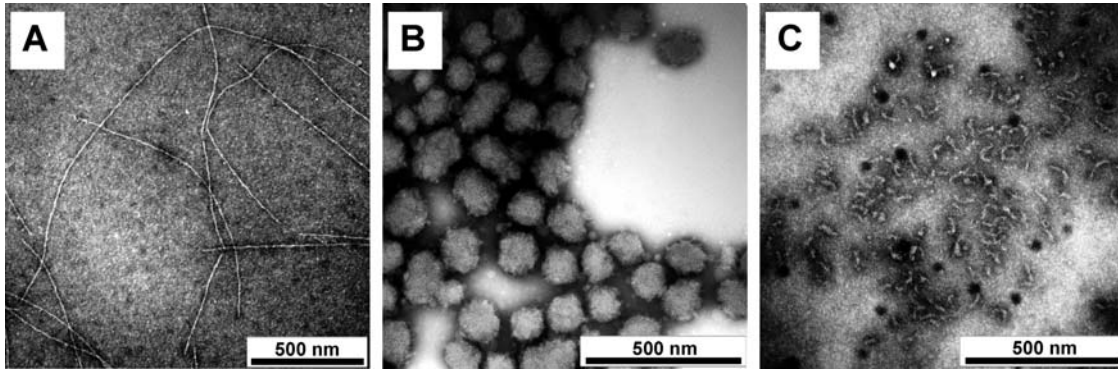
Figure 1. TEM micrographs of βlg aggregates obtained upon heating a 1 wt % protein solution at different pHs: (A) rod-like aggregates obtained at pH 2.0; (B) spherical aggregates obtained at pH 5.8; (C) worm-like primary aggregates obtained at pH 7.0.

anionic surfactant SDS were followed using an isothermal titration calorimeter (CSC4200, Setaram, France). Aliquots of 10 μL of SDS 1 wt % at pH 3.0 were injected sequentially into a 1.5 mL titration cell initially containing either MilliQ water at pH 3.0 (blank) or 0.1 wt % β-lactoglobulin aggregates solution adjusted to pH 3.0. The measurements were performed at room temperature (25 $\pm$ 0.5 °C). The titration cell was continuously stirred at around 300 rpm. A series of 24 injections of 10 μL was performed with an equilibration time of 5 min between each injection. The blank was subtracted from raw data. The molar ratio of SDS to β-lactoglobulin aggregates to obtain complete saturation of the positives charges of β-lactoglobulin aggregates was determined. The measurements were carried out in duplicate for each type of β-lactoglobulin aggregates.

3. Theoretical Background

3.1. Static Light Scattering (SLS). The excess reduced scattering intensity R_θ was determined as a function of the scattering angle θ and the protein concentration C. The data were analyzed using the Zimm procedure and modifications according to Berry and Guinier approximations, using the Debye equation

$$\frac{KC}{R_\theta} = \frac{1}{M_w}\left(1 + \frac{q^2 R_g^2}{3}\right) + 2A_2 C + ... \tag{3}$$

with K being the optical contrast of the instrument, C is the concentration of the sample, R_θ is the Rayleigh ratio of the sample, M_w is the molecular weight of the particle, q is the scattering vector, R_g is the radius of gyration, and A_2 is the second virial coefficient. The optical contrast of the instrument K is calculated as follows

$$K = \frac{1}{N_A}\frac{4\pi^2 n_0^2}{\lambda_0^4}\left(\frac{dn}{dc}\right)^2 \tag{4}$$

with N_A, the Avogadro constant, λ_0, the wavelength of the light in the vacuum, n_0, the refractive index of the solvent, and dn/dc, the differential refractive index increment.

In the case of 3D cross-correlation light scattering, R_θ was corrected for multiple scattering and the transmission, as described in ref 47.

3.2. Dynamic Light Scattering (DLS). In dynamic light scattering a time correlation function (TCF) of the scattering intensity is measured which is given as

$$g_2(t,q) = \frac{\langle i(0)i(t)\rangle}{\langle i(0)\rangle^2} \tag{5}$$

in which $i(0)$ and $i(t)$ are the scattering intensities at time $t = 0$ and at a certain delay time t.

In dilute solutions $g_2(t,q)$ can be expressed in terms of the normalized electric field correlation function $g_1(q,t)$ using Siegert's equation

$$g_2(t) = 1 + \beta|g_1(t)|^2 \tag{6}$$

where the coefficient β depends on the quality of the coherence. When monomodal fiber optics is used, β is close to the theoretical value of 1.

In the case of a monodisperse system of particles and for short delay times $g_1(t)$ is well approximated by a single-exponential decay

$$g_1(t) = \exp(-\Gamma(q)t) \quad \text{if} \quad \Gamma(q)t < 1 \tag{7}$$

This decay time is related to an apparent mutual diffusion coefficient

$$\Gamma(q) = q^2 D_{app}(q,c) \tag{8}$$

The double extrapolation of $D_{app}(q,c)$ to $c = 0$ and $q = 0$ gives the translation diffusion coefficient from which the hydrodynamic radius R_h is determined using the Stokes−Einstein equation

$$R_h = \frac{k_B T}{6\pi\eta_s D_{app}} \tag{9}$$

with k_B, Boltzmann's constant, T, absolute temperature, and η_s, the solvent viscosity.

For polydisperse systems, $g_1(t)$ is given by an integral equation

$$g_1(t) = \int_0^\infty G(\Gamma)e^{-\Gamma t}d\Gamma \tag{10}$$

where $G(\Gamma)$ is the normalized distribution function of the decay rates.

A commonly used technique to analyze eq 10 is the method of cumulants, which is based on a series expansion of $\ln(g_1(t))$:

$$\ln g_1(t) = -\bar{\Gamma}t + \frac{\mu_2}{2}t^2 - \frac{\mu_3}{3!}t^3 + ... \tag{11}$$

At $q = 0$, the first cumulant yields the z average of the diffusion coefficient and the second cumulant is a measure of polydispersity (relative standard deviation, σ).

4. Results and Discussion

4.1. Global Solution Properties of βlg Heat-Induced Aggregates. Figure 1 presents the TEM micrographs for the βlg aggregates obtained at the different pH conditions considered. At very acidic conditions (pH 2.0, Figure 1a), thin, rod-

4

Table 3. Characterization of Molecular Weight, Radius of Gyration, Hydrodynamic Radius, ρ-Parameter, and Polydispersity of βlg Heat-Induced Aggregates Obtained at pH 5.8 and 7.0

pH$_{preparation}$	pH$_{measurement}$[a]	M_w (g·mol^{-1})	R_g (nm)	R_h (nm)	ρ	polydispersity
5.8	5.8	4.60×10^8	60	120	0.50	0.3
7.0	7.0	2.5×10^5	15	14	1.1	0.2
7.0	3.0	2.7×10^5	22	16	1.4	0.2

[a] The light scattering measurements were carried out both at the pH at which the aggregates were prepared and at pH 3.0. For the aggregates prepared at pH 5.8, no difference in size and conformation of the aggregates was observed when the pH was decreased to pH 3.0 and for that reason the corresponding data are not shown.

Figure 2. Scattering wave vector dependency of I/K_c (determined by USALS, SLS and SANS) for rod-like βlg aggregates prepared by heat treatment of 1 wt % monomer solution. The solid line at high q-values is a model fit by the cylindrical form factor which gives the value of the rod's cross-section.

like aggregates with the contour lengths of the order of 1−10 μm are observed in agreement with other literature reports.[5,13,14,35,36] The aggregates are very rigid, as suggested by the presence of perfectly straight segments in the range of 300−800 nm observed along the same individual aggregates. The shape of the aggregates obtained at pH 5.8 (Figure 1b), on the other hand, is very different, indicating very compact and spherical-like aggregates, with a relatively monodisperse and narrow size distribution centered at about 150 nm. Finally, Figure 1c, shows the structure of aggregates obtained at neutral pH 7.0: short, worm-like primary objects with end-to-end distance below 100 nm and a cross-section of around 6 ± 1 nm are observed.

To gain further insight on the global structure of βlg aggregates prepared in dilute regime ($c_{monomer} < c_{gel}$) at the various pH conditions, and to study the parameters that describe the average behavior over the entire particle, including the gyration and hydrodynamic radii, static, and dynamic light scattering was carried out in highly diluted conditions for aggregates obtained at pH 5.8 and 7.0. Indeed, previous work[13,14] on thermal denaturation/aggregation of βlg at pH 2.0 indicated formation of extremely large and polydisperse, yet stable, aggregates with an overall conformation of semiflexible chains at large length scales and a rod-like internal structure at lower length scales. The magnitude of the particle size in this case is out of the length scale probed by light scattering.

As can be immediately recognized from Table 3, soluble aggregates with very different sizes and molar masses were obtained. Because one of the goals of the present study is to investigate the influence of SDS on the aggregates at pH 3.0, that is, when strong electrostatic interactions are expected, the light scattering measurements were carried out both at the pH at which aggregates were prepared, and at pH 3.0. For the aggregates prepared at pH 5.8, which is close to the IEP, little to no difference in the size and conformation of aggregates was recorded when the pH was decreased to 3.0 (data not shown). This suggests rather compact aggregates, whose conformation is less sensitive to the increase of total charge density, in agreement with other observations.[39,40] In the case of aggregates prepared at pH 7.0, a more extended conformation was observed at pH 3.0, consistently with increased internal electrostatic repulsions.

From the combination of static and dynamic light scattering data, an approximate estimation of the shapes of the aggregates is possible. The ratio of the radius of gyration to the hydrodynamic radius corresponds to the so-called ρ-parameter, which is structure-sensitive and is frequently used to characterize polymeric architectures. Given the polydisperse nature of the aggregates, however, the ρ-parameter can be used only to provide a qualitative, approximate interpretation of the shapes of the aggregates. βlg aggregates prepared at pH 7.0 and measured at pH 3.0 gave a value $\rho = 1.4$, which is characteristic
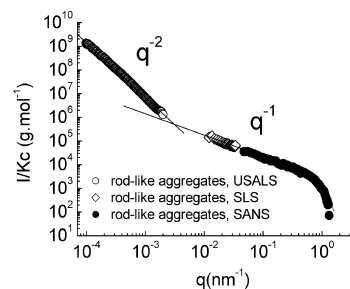
for polydisperse coils in a good solvent. The unexpected lower value of $\rho = 1.1$, at pH 7.0, can probably be attributed to the decreased charge density of the aggregates. In the case of aggregates prepared at pH 5.8, a much smaller value of ρ was obtained, $\rho = 0.56$. For comparison, ρ is expected to be 0.775 for hard-type spheres and 0.35−0.55 for micelle-like aggregates and microgel particles.[48] These findings are again supporting the presence of compact objects with possible structures, such as micellar or microgels with dangling chains at the surface.

Assuming for the βlg aggregates prepared at pH 5.8 a spherical shape, the knowledge of the molar mass M_w of the particle together with the radius of gyration R_g allows one determining the apparent density of the dissolved material based on the following equation for homogeneous spheres

$$d_{app} = \frac{M_w}{N_A(4\pi/3)R_g^3} \quad (12)$$

which gives an apparent density of 0.53 g·mL^{-1}. Aggregates dried by spray-drying technique gave a density of 1.5012 g·mL^{-1}. These data suggest a high swelling ratio equal to 2.8 without a structural loss in agreement with the predicted microgel behavior.

4.2. Structure of βlg Aggregates. To gain information on the internal structure, the three types of aggregates were further investigated by SANS and SAXS. For the form factor analysis, the scattered light intensity and neutron/X-ray scattering intensities measured at the same concentration C were combined to cover a q regime from 8×10^{-3} nm^{-1} ≤ q ≤ 1 nm^{-1}. For absolute scattering intensities, the SANS and SAXS data were shifted to absolute SLS data.

4.2.1. βlg Aggregates Prepared at pH 2 (Figure 2). Given the large size of the aggregates prepared at pH 2, the Guinier regime in reciprocal space locates at q regions beyond those probed by visible light. Thus, TEM was the only technique able to probe the entire dimensions of the aggregates prepared at pH 2 (see Figure 1a). Nonetheless, more details on the internal shape of aggregates could be obtained using USALS, SANS and SAXS. In the q-range covered by USALS (10^{-4} nm^{-1} < q < 10^{-3} nm^{-1}) shorter sections of the aggregates are seen corresponding to distances $r_{ij} < R_g$ but still much larger than the Kuhn segment length. The scattering intensity was measured in arbitrary units at a number of selected scattering angles and normalized by the scattering intensity at scattering angle zero. This normalized angular dependence on a double logarithmic scale gave a straight line and its slope allowed the determination of fractal dimension d_f. A slope of -2 was obtained, which is the negative fractal dimension of a linear Gaussian chain. This is in agreement with the folding behavior of the rod-like
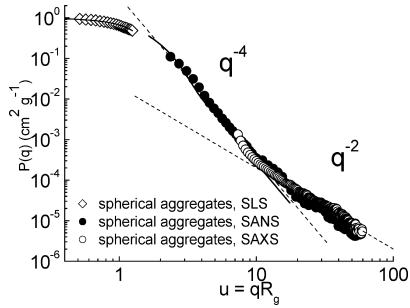
Figure 3. Form factor (determined by USALS, SLS, and SANS) for spherical βlg aggregates obtained by heat treatment of 1 wt % monomer solution. The dashed lines highlight q^{-4} and q^{-2} dependences. Values used for R_g in the qR_g axis are those given in Table 3.

Figure 4. The form factor (determined by USALS, SLS, and SANS) for worm-like primary βlg aggregates generated by heat treatment of 1 wt % monomer solution. Self-avoiding flexible coil fractal dimension (−1.7) is found at intermediate q (solid line) and cross-section information can be obtained at large q by applying Porod's equation (dashed line). The dotted line highlights the $q^{-1.7}$ dependence. Values used for R_g in the qR_g axis are those given in Table 3.

aggregates observed by TEM at length scales larger than 1 μm. Combining middle angle light scattering and SANS (2×10^{-3} nm$^{-1} < q < 10^{-1}$ nm^{-1}), distances smaller than the Kuhn segment length of the rod-like aggregates could be investigated, and the behavior of a rod with the asymptotic slope equal to −1, that is, $d_f = 1$, was recovered. It is clear that there is a crossover in the q-range where the transition between a flexible chain and a rod occurs, but because the USALS data are in arbitrary units, the position of the crossover point cannot be resolved, and thus, the exact Kuhn length of the rod-like aggregates cannot be determined. This, however, has to be found between 380 and 1980 nm based on the q extremes settled by the last point of USALS and first point of SLS. At the highest q-region investigated (10^{-1} nm$^{-1} < q < 1.2$ nm^{-1}), the last points of the SANS deviate from the −1 slope, as this is the region corresponding to length scales below the Kuhn length and of the order of the cross-section of the rod-like aggregates. For infinitely rod-like particles, Porod derived the following approximate formula, which allows the determination of the rod cross-section[49]

$$\frac{I}{K_c} = \frac{m\pi}{q} \cdot \exp\left(-\frac{q^2 R_c^2}{2}\right) \tag{13}$$

where R_c is the radius of gyration of the cross-section and m is the molar mass per length unit. For a cylinder, the gyration radius R_c is related to the cylinder radius R by

$$R = R_c \sqrt{2} \tag{14}$$

The analysis of the high q end of the scattering curve using the Porod's equation gave a value $R_c = 1.5$ nm which corresponds to $R = 2.12$ and to a cross-section of 4.24 nm. This is again in agreement with the microscopy results (see also Table 3) and other literature reports.

4.2.2. βlg Aggregates Prepared at pH 5.8 (Figure 3). To represent the form factor, the dimensionless parameter $u = qR_g$, was preferred over the scattering vector q. As we worked at low concentrations, the initial part of the scattering curve (7×10^{-3} nm$^{-1} < q < 7 \times 10^{-2}$ nm^{-1}) in double logarithmic coordinates represents the Guinier plot, which allows the determination of the radius of gyration. For the intermediate q regime (4.5×10^{-2} nm$^{-1} < q < 2.5 \times 10^{-1}$ nm^{-1}), the scattering behavior was successfully described by the model of polydisperse hard spheres (see Appendix), where a polydispersity of 30% was used, as measured by separate DLS measurements. Compared to DLS finding, however, a smaller radius, $R = 50$ nm, had to be used for a good fitting. The reasons for this difference are understood as follows. First, we note that the q^{-4}

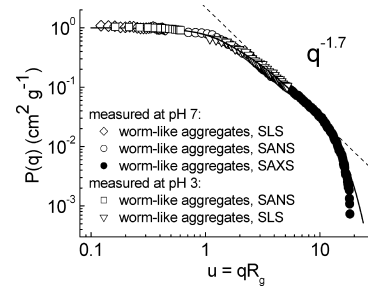power law obtained in the fit, frequently called the Porod law, indicates that the aggregates are densely packed objects and sharp boundaries occur between the scattering objects and the surrounding solvent. Then we recall that the analysis of the ρ-parameter suggested a micelle- or a microgel-like structure with dangling chains at the surface of aggregates. Mobility of the side chains on the aggregates surface is expected to provide to the particles a larger apparent size than what was estimated by the fitting of our SANS data recorded in D$_2$O in static conditions. To this end, experimental studies on the structure of the protein−solvent interface have further demonstrated that the higher scattering length density of D$_2$O by comparison to that of protein, determines the formation of a denser hydration layer at the protein surface, which reduces the apparent size of the particles.[50]

At larger q-values ($q > 0.25$ nm^{-1}), the scattering curve flattens and approaches a slope of −2. The length scales probed in this q-regime correspond to the internal structure of the spherical aggregates, typically in the order of a few monomers, and thus, this slope might be indicative of the self-assembly of the monomers within the sphere-like aggregates.

4.2.3. βlg Aggregates Prepared at pH 7 (Figure 4). In the low q-regime (7×10^{-3} nm$^{-1} < q < 7 \times 10^{-2}$ nm^{-1}), the scattering intensity was analyzed by the classical Guinier method to obtain the radius of gyration. The ρ-parameter indicated linear chain behavior, and accordingly, the TEM showed worm-like chain aggregates, therefore, the overall conformation of aggregates should correspond to weakly bended linear chains. It is to be expected that, at higher concentrations and higher ionic strengths than those used in the present work, branching points along the main backbone of the aggregates would start to appear, leading to branched fractal objects, in accordance with previous work.[7] In the present case, given the lower concentration and ionic strength used, no evidence is found for such branching. Therefore, the scattering curve at low and intermediate q (7×10^{-2} nm$^{-1} < q < 7 \times 10^{-1}$ nm^{-1}) was fitted by the model of polydisperse coils

$$P(u) = \frac{1}{1 + \frac{u^2}{3}} \tag{15}$$

with the mention that, in the case of short chains, eq 15 remains approximately valid for all types of particle architectures because it converges to the general Guinier expression. Thus, differences in architecture become detectable at $u = qR_g > 3$. The asymptotic slope in this model is −2, which is the negative fractal dimension of a Gaussian chain. A separate and more
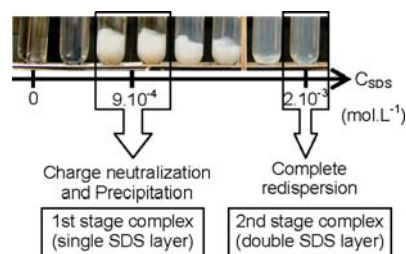
Figure 5. Macroscopic behavior of 0.1 wt % rod-like βlg aggregates after complex formation with SDS at different surfactant concentrations, pH 3.0 and 25 °C.

Figure 6. Electrophoretic mobility of 0.1 wt % βlg aggregate and native βlg protein as a function of SDS molar concentration for the different βlg−SDS complexes obtained at pH 3.0 and 25 °C.

careful estimation of the experimental asymptotic slope, however, gave a value of −1.7, in agreement with data from the literature.[51] This fractal dimension is exactly that expected for self-avoiding random walks, which is again in perfect agreement with the findings based on TEM and the prediction of coils in a good solvent, as determined by the ρ-parameter analysis. The steep dependence observed at large q-values ($q > 0.7$ nm^{-1}) was fitted by Porod's equation and the cross-section of the linear chains was found to be equal to 5 nm, again, in very close agreement with the values found by TEM analysis at 6 ± 1 nm.

Very similar scattering curves were found at pH 7 and pH 3 (Figure 4), indicating that the change of pH has only a weak influence on the aggregate conformation. The same results were obtained for aggregates prepared at pH 2 and pH 5.8 (data not shown).

4.3. Complexation of βlg Aggregates with SDS at pH 3. As anticipated, βlg is capable of binding to a wide variety of organic compounds (retinol, vitamins, lipids, surfactants) through electrostatic or hydrophobic interactions.[52−54] When the monomer is charged oppositely to the surfactant ions, the number of bound ligands is much higher than for the case of nonionic surfactant or surfactants with the same charge. Specific ion-pair electrostatic interactions usually correspond to low molar ratios of surfactant to the globular protein (maximum 2:1) and further binding of surfactant anions might be accompanied by conformational change in the protein and cooperative binding.

For a given surfactant, its binding depends on protein surface charge density and follows the mass action equilibrium. Thus, it can be assumed that, in the case of noncooperative binding, the mean number of bound surfactant molecules per molecule of protein aggregate will increase with the concentration of free surfactant.

Prior to titration, charged βlg aggregates are stabilized by electrical double layer repulsions. To ensure small interference effects, in the study, the protein aggregate solutions were diluted to 0.1 wt % solids. This high dilution allowed performing all binding experiments at very low surfactant concentrations, below the critical micelle concentration (CMC) of SDS, determined to be 8 mM at pH 3 by conductometric titration (results not shown).

4.3.1. Binding of SDS to βlg Aggregates Investigated by Electrophoretic Mobility and ITC Measurements. The complexation steps between βlg aggregates and SDS have been followed, as seen in Figure 5. A two-step complexation could be observed: the first step corresponding to the precipitation of the complexes and a second step corresponding to total redispersion of the precipitates.

In Figure 6, electrophoretic mobility was plotted against the concentration of SDS, and the same dependence was obtained for all the investigated samples and the native βlg protein. No different behavior can be resolved for different topologies, which
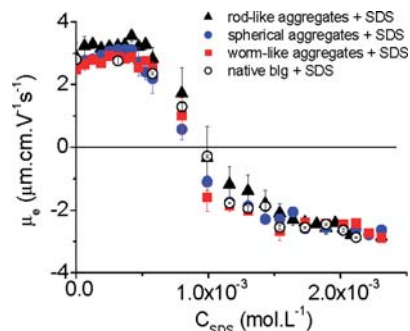
suggests similar electrostatic coupling behavior during the neutralization with SDS. A slight decrease of the electrophoretic mobility with the pH of preparation was observed. This behavior can tentatively be explained by the different topologies of aggregates obtained at various pHs. At pH 2.0, because of the linear aggregation mechanisms, all the monomers will contribute to the overall charge of the aggregate, while at pH 5.8, the monomers are closely packed together and form a compact sphere whose observable overall charge is provided only by the external layers of monomers.

Table 4 summarizes the binding ratios extracted from electrokinetic measurements when electrophoretic mobility becomes zero.

The shape of the electrophoretic mobility curves indicated that SDS anions are bound to βlg aggregates in three stages:

1. The first step corresponds to the first plateau from the electrophoretic mobility curve in which SDS adsorption and charge neutralization occur only in limited amount, as revealed by the unaffected overall electrophoretic mobility. Because both bound and unbound SDS molecules should be found at equilibrium, and only the bound molecules are expected to effectively decrease the total electrophoretic mobility, this plateau regime suggests that the binding equilibrium constant is relatively small and that fairly high concentrations of SDS are needed to push the equilibrium concentrations toward a high amount of bound surfactant.

2. A second step, at higher SDS concentrations, corresponds to the decrease of the electrophoretic mobility, in which the surfactant complexes with the aggregates, neutralizing the total charge at the protein aggregate surface. At the concentration corresponding to the neutral electrophoretic mobility (ca. 9×10^{-4} mol·L^{-1}), most of the aggregates−SDS complexes are found to precipitate. This is in agreement with the classical Derjaguin−Landau−Verwey−Overbeek theory, according to which uncharged proteins tend to aggregate due to van der Waals and hydrophobic attractions.

3. A third binding step taking place upon further increase in SDS concentration corresponds to an inversion of the sign of the overall electrophoretic mobility. Remarkably, in this regime of SDS concentration, the precipitates are found to fully redisperse in water, stabilized into colloidal dispersions of SDS−βlg aggregates complexes. For example, at concentrations of SDS $\sim 2 \times 10^{-3}$ mol·L^{-1}, which is still below the CMC and, thus, where the only contribution to overall electrophoretic mobility is given by SDS−βlg aggregates complexes, the aggregates have acquired a high amount of total negative charge capable of redispersing the complexes in water. At high concentration regime of SDS ($>10^{-3}$ mM), the binding of the surfactant is expected to occur by hydrophobic interactions via

Table 4. Molar Ratio of SDS/βlg Aggregates and SDS/Native βlg To Obtain a Neutrally-Charged Precipitate for the Different Conditions of Preparation

βlg type	rods	spheres	worm-like	native protein
SDS/βlg aggregate molar ratio[a]	8.9×10^4:1	6.2×10^5:1	3.4×10^2:1	50:1

[a] For the sphere-like and worm-like βlg aggregates, the number of moles was calculated as the ratio of the initial mass of protein to the molar mass of the corresponding aggregate, as determined by SLS (see Table 3). To estimate the average molar mass of the rods, first the aggregation number was obtained dividing the average length (10 μm) by the monomer diameter (4 nm), then this aggregation number was multiplied by the molar mass of the monomer (M_w = 18400 g·mol^{-1}).

the merging of hydrophobic domains found on the protein surface and the SDS alkyl tails. The increased charge at the complex surfaces resulting from hydrophobic interactions is understood to be the main mechanism leading to redispersion of the aggregates. As hydrophobic interactions are noncovalent and relatively weak, they might rapidly dissociate. Further experiments are needed to prove the stability of the redispersed SDS−βlg aggregates complexes.

ITC is a highly sensitive technique generally used to study protein−ligand interactions in dilute aqueous solutions, both from thermodynamic and kinetic points of view.[55] More specifically, the heat of interaction during the titration of a protein solution against the concentration of the ligand is measured. Enthalpy variations (i.e., gain and/or loss) are calculated as the heat released per mole of injected ligand and can be interpreted in terms of various molecular events, for example, specific binding, cooperative binding, protein unfolding, or protein aggregation. In general, it is difficult to assign precise molecular events to enthalpy changes measured in calorimetry measurements because many different physicochemical phenomena contribute to the overall measured signal, for example, various kinds of association−disassociation processes and conformational changes.

Figure 7a shows the raw calorimetric data obtained during titration, while Figure 7b corresponds to the binding isotherms of SDS on the aggregate surface. As is apparent from both figures, in the present case, ITC was sufficiently accurate to probe the strong electrostatic protein−surfactant interactions that take place before precipitation, but it was much less-sensitive to describe the hydrophobic interactions that occur after the precipitation point. This is to be expected by considering the very different specific enthalpy associated to ionic and hydrophobic interactions.[56] Because the ratio of free/bound SDS molecules at any specific concentration of SDS remains unknown at this stage, the binding isotherms cannot be plotted versus the number of moles of bound SDS, and the equilibrium binding constant cannot be determined.

Relatively large exothermic peaks were observed when the surfactant solution was injected into the reaction cell in the initial titration steps (see Figure 7a). The exothermic character was believed to be due to the strong electrostatic interactions between the protein aggregates and the surfactant. As the available sites become progressively occupied during titration, the exothermicity of the peaks decreases and eventually saturates. This can be understood by considering that as complex formation proceeds, more and more unbound free surfactant is needed to drive the equilibrium toward an increased complexation rate, resulting progressively in less and less SDS molecules contributing to the ionic enthalpic gain. Apparently, the number of injections required for achieving the saturation (and thus the same SDS concentration) seems to be the same for different aggregates. To explain this behavior one has to take into account that for all solutions the same initial concentration of monomer was considered, and that, the thermally induced aggregation resulted in solutions containing the same weight of protein but a different number of moles of βlg aggregates.
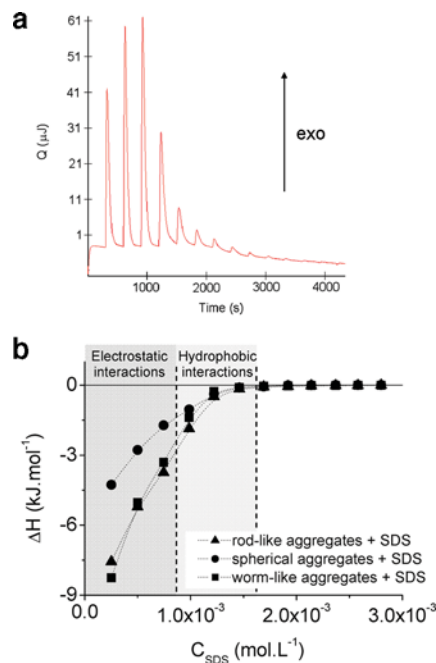

Figure 7. (a) Heat released versus time during the binding process of 0.1 wt % rod-like βlg aggregates with SDS as measured by ITC measurements at 25 °C. (b) Binding enthalpies upon complex formation of 0.1 wt % βlg aggregates with SDS as a function of SDS concentration. The boundary between the two regimes (electrostatic vs hydrophobic interactions) corresponds to the concentration at which complete charge neutralization of the aggregate−SDS complexes is found (see Figure 6).

4.3.2. Probing β-Lactoglobulin Aggregates−SDS Complexes by TEM. Several attempts were made to probe the structure of the β-lactoglobulin−SDS complexes. In particular, due to their extremely high aspect ratio and very small cross-section, rod-like aggregates constitute an ideal system to detect systematic increases in the cross-section arising from complex formation with SDS.

First attempts consisted in detecting by SAXS the increase in the cross-section of the rod-like aggregates. Unfortunately, very dilute solutions at which the added SDS is present below the CMC were too diluted to yield sufficiently defined scattered signal. More dense solutions resulted in coexistence of complexes and SDS micelles, which smeared the q-region corresponding to the rod-like cross-section.

In a further attempt to characterize the cross-section of the rod-like aggregates before and after complex formation with SDS, we used TEM. Figure 8a,b give typical TEM micrographs obtained by casting pH 3.0 water dispersions of rod-like aggregates before and after complex formation with SDS, respectively, onto TEM copper grids, as described in the Materials and Methods. By performing a systematic measurement of the rod-like aggregates cross-section, diameters of 5.2 ± 1.1 nm (20 samples) and 12 ± 3.1 nm (40 samples), are found for the uncomplexed and complexed aggregates, respectively. Assuming core−shell geometry for the complex, the
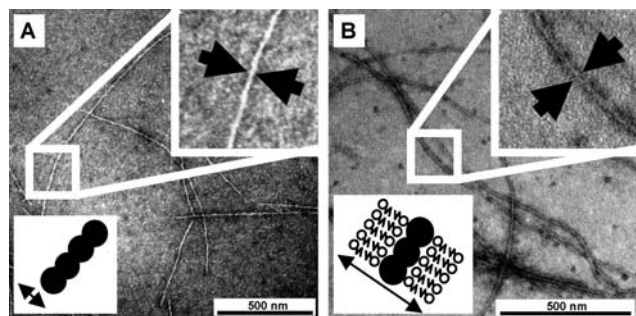
8

Figure 8. TEM micrographs of rod-like βlg aggregates (A) before complex formation and (B) after complexation with SDS. The insets show a highly idealized arrangement of the aggregates and surfactant before and after complex formation.
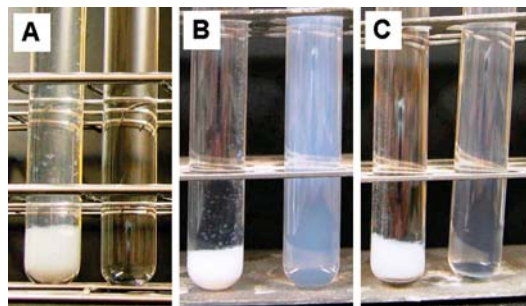

Figure 9. βlg−SDS complexes formed at 0.1 wt % adjusted to IEP of the protein aggregates: (A) rod-like aggregates; (B) spherical aggregates; and (C) worm-like primary aggregates. For each type of aggregate, the left tube contains the uncomplexed aggregates and the right tube contains the same aggregates after complex formation with a double layer of SDS. The SDS double layer protects the aggregates from macroscopic precipitation at IEP.

thickness of the shell is found to be at 6.8/2 = 3.4 nm. This compares perfectly with twice the contour length of fully stretched SDS molecules,[57] suggesting that the SDS molecules adopt a head-to-head configuration around the β-lactoglobulin aggregates.

Although a SDS bilayer can directly be imaged only for the rod-like aggregates due to the high relative increase in cross-section, this behavior is expected to be similar for complexes generated between SDS and both the spherical and the worm-like aggregates. The more spectacular evidence in favor of this hypothesis is that, when exposing the complexes of SDS with spherical aggregates and worm-like primary aggregates to pH corresponding to the IEP point of the aggregates, the dispersions remain stable without precipitation, as rod-like aggregate−SDS complexes also do. Figure 9 compares the dispersions observed at the isoelectric pH for the three types of heat-induced protein aggregates and their complexes with SDS: a transparent, homogeneous dispersion is observed for all the complexes (for spherical aggregates, the slight turbidity is related to the presence of 200 nm large objects, independently of pH). Thus, the presence of a shielding, protective SDS bilayer confers a new, unobserved property to the protein aggregates, such as their stability against pH, especially at the IEP.

5. Conclusions

We have investigated the structure of heat-induced β-lactoglobulin aggregates prepared at different pH conditions, and we have studied the interactions at pH 3.0 of these aggregates with sodium dodecyl sulfate, an anionic surfactant.

By combining different scattering techniques from different sources (light, neutrons, and X-rays), we could probe different length scales in the reciprocal space, yielding the scattering form factors for aggregates obtained at different pHs. It was then possible to show that, by increasing the pH from 2.0 to 5.8 to 7.0, rod-like, sphere-like, and worm-like aggregates could be obtained with different gyration radii, hydrodynamic radii, internal densities, and fractal dimensions.

Particular emphasis was given to the study of the interactions of these aggregates with anionic surfactants. By combining electrophoretic mobility and isothermal titration calorimetry, different regimes in the complex formation between the aggregates and the anionic surfactant could be found, complex formation proceeding first by ionic interactions and then by hydrophobic interactions, when increasing concentrations of anionic surfactant were used. As expected, in the intermediate concentration regime, corresponding to the complete neutralization of charges on the protein aggregate surfaces, the complexes precipitated, due to van der Waals and hydrophobic attractions. Surprisingly, however, at larger concentrations of SDS, the complexes could be completely redispersed in water and this, even at pH values identical at the IEP of the aggregates. This effect was understood to depend on the presence of a protective ionic surfactant double layer around the protein aggregates.

Direct evidence of the double layer was given by the negative electrophoretic mobility at high surfactant concentration and by the visualization by transmission electron microscopy of an increased cross-section for the rod-like protein aggregate−surfactant complexes. The increase in the cross-sectional shell thickness was perfectly consistent with a tail to tail configuration of the surfactant molecules.

Appendix

Influence of polydispersity on the form factor of hard spheres: The form factor for monodisperse hard spheres can be written as

$$P(u)_{\text{hard-sphere}} = \left[\frac{3}{X^3}(\sin X - X \cos X)\right]^2 \quad \text{where}$$

$$X = qR_{\text{hard-sphere}} \quad \text{(A1)}$$

For calculating the influence of the polydispersity on the form factor the following formula is considered

$$\int_{-\infty}^{+\infty} \varpi(R)P(u)\mathrm{d}R \cong \sum_{j=1}^{n} h_j(R)P_j(u) \quad \text{(A2)}$$

The radii distribution was determined, as in ref 58.

References and Notes

(1) Qin, B. Y.; Bewley, M. C.; Creamer, L. K.; Baker, H. M.; Baker, E. N.; Jameson, G. B. *Biochemistry* **1998**, *37*, 14014–14023.

(2) Brownlow, S.; Cabral, J. H. M.; Cooper, R.; Flower, D. R.; Yewdall, S. J.; Polikarov, I.; North, A. C. T.; Sawyer, L. *Structure* **1997**, *5* (4), 481–495.

(3) Fogolari, F.; Ragona, L.; Liccaiardi, S.; Romagnoli, S.; Michelutti, R.; Ugolini, R.; Molinari, H. *Proteins: Struct., Funct., Genet.* **2000**, *39* (4), 317–330.

(4) Aymard, P.; Durand, D.; Nicolai, T. *Int. J. Biol. Macromol.* **1996**, *19*, 213–221.

(5) Veerman, C.; Ruis, H.; Sagis, L. M. C.; van der Linden, E. *Biomacromolecules* **2002**, *3* (4), 869–873.

(6) Veerman, C.; Baptist, H.; Sagis, L. M. C.; van der Linden, E. *J. Agric. Food Chem.* **2003**, *51*, 3880–3885.

(7) Le Bon, C.; Nicolai, T.; Durand, D. *Macromolecules* **1999**, *32*, 6120–6127.

(8) Mahmoudi, N.; Mehalebi, S.; Nicolai, T. *J. Agric. Food Chem.* **2007**, *55*, 3104–3111.

(9) Lefebvre, J.; Renard, D.; Sanchez-Gimeno, A. C. *Rheol. Acta* **1998**, *37*, 345–357.

(10) Pouzot, M.; Nicolai, T.; Visschers, R. W.; Weijers, M. *Food Hydrocolloids* **2005**, *19*, 231–238.

(11) Pouzot, M.; Durand, D.; Nicolai, T. *Macromolecules* **2004**, *37* (23), 8703–8708.

(12) Vreeker, R.; Hoekstra, L. L.; den Boer, D. C.; Agterof, W. G. M. *Food Hydrocolloids* **1992**, *6* (5), 423–435.

(13) Aymard, P.; Nicolai, T.; Durand, D.; Clark, A. *Macromolecules* **1999**, *32*, 2542–2552.

(14) Arnaudov, L. N.; de Vries, R.; Ippel, H.; van Mierlo, C. P. M. *Biomacromolecules* **2003**, *4*, 1614–1622.

(15) Bolder, S. G.; Hendrickx, H.; Sagis, L. M. C.; van der Linden, E. *J. Agric. Food Chem.* **2006**, *54*, 4229–4234.

(16) Roefs, S. P. F. M.; De Kruif, C. G. *Eur. J. Biochem.* **1994**, *226*, 883–889.

(17) Galani, D.; Owusu Apenten, R. K. *Int. J. Food Sci. Technol.* **1999**, *34*, 467–476.

(18) Surroca, Y.; Haverkamp, J.; Heck, A. J. R. *J. Chromatogr., A* **2002**, *970*, 275–285.

(19) Havea, P.; Carr, A. J.; Creamer, L. K. *J. Dairy Res.* **2004**, *71*, 330–339.

(20) Krebs, M. R. H.; Devlin, G. L.; Donald, A. M. *Biophys. J.* **2007**, *92*, 1336–1342.

(21) Bromley, E. H. C.; Krebs, M. R. H.; Donald, A. M. *Eur. Phys. J. E* **2006**, *21* (2), 145–152.

(22) O'Kennedy, B. T.; Mounsey, J. S.; Murphy, F.; Perquera, L.; Mehra, R. *Milchwissenschaft* **2006**, *61* (4), 366–369.

(23) Schokker, E. P.; Singh, H.; Pinder, D. N.; Creamer, L. K. *Int. Dairy J.* **2000**, *10* (4), 233–240.

(24) Stauffer, D. *Introduction to Percolation Theory*; Taylor & Francis: London, 1985.

(25) Dauoud, M.; Martin, J. E. Fractal Properties of Polymers. In *The Fractal Approach to Heterogeneous Chemistry*; Avnir, D., ed.; Wiley & Sons: New York, 1989.

(26) Mezzenga, R.; Schurtenberger, P.; Burbidge, A.; Michel, M. *Nat. Mater.* **2005**, *4*, 729–740.

(27) Ghosh, S.; Banerjee, A. *Biomacromolecules* **2002**, *3* (1), 9–16.

(28) Ponomarenko, E. A.; Waddon, A. J.; Bakeev, K. N.; Tirrell, D. A.; MacKnight William, J. *Macromolecules* **1996**, *29*, 4340–4345.

(29) Sjögren, H.; Ericsson, C. A.; Evenäs, J.; Ulvenlund, S. *Biophys. J.* **2005**, *89*, 4219–4233.

(30) Deo, P.; Deo, N.; Somasundaran, P.; Moscatelli, A.; Jockusch, S.; Turro, N. J.; Ananthapadmanabhan, K. P.; Francesca Ottaviani, M. *Langmuir* **2007**, *23*, 5906–5913.

(31) Santos, S. F.; Zanette, D.; Fischer, H.; Itri, R. *J. Colloid Interface Sci.* **2003**, *262*, 400–408.

(32) Kelley, D.; McClements, D. J. *Food Hydrocolloids* **2003**, *17*, 73–85.

(33) Magdassi, S.; Vinetsky, Y.; Relkin, P. *Colloids Surf., B* **1996**, *6*, 353–362.

(34) Majhi, P. R.; Ganta, R. R.; Vanam, R. P.; Seyrek, E.; Giger, K.; Dubin, P. L. *Langmuir* **2006**, *22*, 9150–9159.

(35) Renard, D.; Lefebvre, J. *Int. J. Biol. Macromol.* **1992**, *14*, 287–291.

(36) Kavanagh, G. M.; Clark, A. H.; Ross-Murphy, S. B. *Int. J. Biol. Macromol.* **2000**, *28*, 41–50.

(37) Schmitt, C.; Bovay, C.; Rouvet, M.; Shojaei-Rami, S.; Kolodziejczyk, E. *Langmuir* **2007**, *23*, 4155–4166.

(38) Renard, D. Université de Nantes, France, 1994.

(39) Schmitt, C.; Vuilliomenet, A.-M.; Bovay, C.; Rouvet, M.; Bovetto, L.; Barbar, L.; Sanchez, C. 2008, in preparation.

(40) Donato, L.; Schmitt, C.; Bovetto, L. 2008, in preparation.

(41) Arnaudov, L. N. Wageningen Universiteit, The Netherlands, 2005.

(42) Cipelletti, L.; Weitz, D. A. *Rev. Sci. Instrum.* **1999**, *70*, 3214–3221.

(43) Bhat, S. K.; Moitzi, C.; Schurtenberger, P. 2008, in preparation.

(44) Urban, C.; Schurtenberger, P. *J. Colloid Interface Sci.* **1998**, *207*, 150–158.

(45) Cotton, J. P. *Initial Data Treatment, in Neutron, X-ray and Light Scattering: Introduction to an Investigative Tool for Colloidal and Polymeric Systems*; North-Holland: Amsterdam, 1989.

(46) Jacrot, B.; Zaccai, G. *Biopolymers* **1981**, *20*, 2413–2426.

(47) Nicolai, T.; Urban, C.; Schurtenberger, P. *J. Colloid Interface Sci.* **2001**, *240*, 419–424.

(48) Burchard, W. *Adv. Polym. Sci.* **1999**, *143*, 113.

(49) *Small Angle X-ray Scattering*; Academic Press: London, 1982.

(50) Svergun, D. I.; Richard, S.; Koch, M. H. J.; Sayers, Z.; Kuprin, S.; Zaccai, G. *Proceedings of the National Academy of Science*, 1998, Vol. 95, pp 2267−2272.

(51) Durand, D.; Gimel, J. C.; Nicolai, T. *Physica A* **2002**, *304*, 253–265.

(52) Girard, M.; Turgeon, S. L.; Gauthier, S. F. *J. Agric. Food Chem.* **2003**, *51*, 4450–4455.

(53) Guzey, D.; McClements, D. J. *Food Hydrocolloids* **2006**, *20*, 124–131.

(54) Laos, K.; Brownsey, G. J.; Ring, S. G. *Carbohydr. Polym.* **2007**, *67*, 116–123.

(55) Tellinghuisen, J. *J. Phys. Chem. B* **2005**, *109*, 20027–20035.

(56) Hammond, M.; Mezzenga, R. *Soft Matter* **2008**, *4*, 952–961.

(57) Canilho, N.; Kasëmi, E.; Schlüter, A. D.; Ruokolainen, J.; Mezzenga, R. *Macromolecules* **2007**, *40*, 7609.

(58) Stauch, O.; Schubert, R.; Savin, G.; Burchard, W. *Biomacromolecules* **2002**, *3*, 565–578.